RSC Advances

PAPER

View Article Online
View Journal | View Issue

Cite this: *RSC Adv.*, 2018, **8**, 7173

Suppressing self-discharge of Li–B/CoS_2 thermal batteries by using a carbon-coated CoS_2 cathode†

Youlong Xie, Zhijian Liu,* Huilong Ning, Haifeng Huang and Libao Chen

Received 5th December 2017
Accepted 5th February 2018

DOI: 10.1039/c7ra13071f

rsc.li/rsc-advances

Thermal batteries with molten salt electrolytes are used for many military applications, primarily as power sources for guided missiles. The Li–B/CoS_2 couple is designed for high-power, high-voltage thermal batteries. However, their capacity and safe properties are influenced by acute self-discharge that results from the dissolved lithium anode in molten salt electrolytes. To solve those problems, in this paper, carbon coated CoS_2 was prepared by pyrolysis reaction of sucrose at 400 °C. The carbon coating as a physical barrier can protect CoS_2 particles from damage by dissolved lithium and reduce the self-discharge reaction. Therefore, both the discharge efficiency and safety of Li–B/CoS_2 thermal batteries are increased remarkably. Discharge results show that the specific capacity of the first discharge plateau of carbon-coated CoS_2 is 243 mA h g^{-1} which is 50 mA h g^{-1} higher than that of pristine CoS_2 at a current density of 100 mA cm^{-2}. The specific capacity of the first discharge plateau at 500 mA cm^{-2} for carbon-coated CoS_2 and pristine CoS_2 are 283 mA h g^{-1} and 258 mA h g^{-1} respectively. The characterizations by XRD and DSC indicate that the carbonization process has no noticeable influence on the intrinsic crystal structure and thermal stability of pristine CoS_2.

Introduction

Thermal batteries are chemical power supplies which use molten salts as electrolytes and operate in the range from 350 °C to 550 °C. They are activated by employing an internal pyrotechnic source to produce the heat and melt salt electrolytes. The excellent ionic conductivity of molten salts means thermal batteries can work at high output power. Thermally batteries are mainly used as power sources for guided weapon systems due to their harsh-environment endurance, fast-activation and long storage times.[1,2] Metal sulfides with outstanding conductivity have been widely applied to lithium ion batteries, supercapacitors or lithium–sulfur batteries.[3,4] One of them is CoS_2 which is becoming an important cathode material for thermal batteries. Compared with other metal sulfides like FeS_2 and NiS_2, it has the lowest solubility in most molten electrolytes and the highest electronic conductivity. Furthermore, its thermal decomposing temperature is up to 650 °C, which is of great significance for the safety properties of thermal batteries.

Lithium alloys have been used as anode materials for thermal batteries, such as Li–Al, Li–Si, and Li–B alloy. To match with the excellent electrochemical properties of CoS_2 cathode, Li–B alloy anode which has good power property for its outstanding Li activity, is considered to be the best choice. Different from conventional LiCl–KCl eutectic electrolyte, LiF–LiCl–LiBr molten salt system has an ionic conductivity up to 6.52 S cm^{-1}.[5,6] Thus the Li–B/LiF–LiCl–LiBr/CoS_2 couple is now the most suitable assembly for the high-power output thermal batteries. However, the free lithium in Li–B alloy is very easy to dissolve into the electrolytes. Then the dissolved lithium diffuses to the cathode and reacts with cathode materials once thermal batteries are activated, which results in serious self-discharge at discharge. Above phenomenon can be related to the rule that alkali-metal had a considerable solubility in molten alkali halide.[7] The solubility of lithium at LiF–LiCl–LiBr eutectic is between 1 mol% and 2 mol%, which was measured by Watanabe N.[8] The Li activity of the anode has a dramatic influence on increasing the dissolving process and Li–B alloy has much higher Li activity than Li–Si alloy and Li–Al alloy. Therefore the capacity of Li–B/CoS_2 cells is more greatly influenced by the severe self-discharge especially in the case of long operating life thermal batteries. Self-discharge rate of Li–B/LiF–LiCl–LiBr/CoS_2 cells measured by Gao was up to 20 mA cm^{-2},[9] which is almost times more than Li–Si/CoS_2 cells. In addition, a drastic exothermic reaction accompanied with self-discharge reactions, may destroy the battery and cause serious safety issues. So far, performances of Li–B/CoS_2 batteries are still limited by self-discharge.

Various strategies have been employed to address the self-discharge caused by dissolved lithium in Li–B/LiF–LiCl–LiBr/CoS_2 cells. Zeng reported that applying additive of nanometal powder to LiF–LiCl–LiBr electrolytes could effectively suppress the dissolution of lithium anode.[10] Different from Zeng,

State Key Laboratory of Powder Metallurgy, Central South University, Changsha 410083, China. E-mail: csulzj1208@163.com; Tel: +86 13974870130

† Electronic supplementary information (ESI) available. See DOI: 10.1039/c7ra13071f

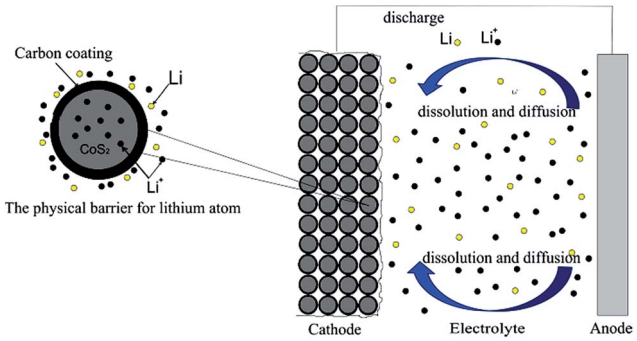

Fig. 1 The influence of modifying CoS_2 cathode materials by the carbon coating at thermal batteries.

preventing direct contact between dissolved lithium and active cathode materials through surface modification may be another promising strategy in solving this problem. Similar strategies have been applied to suppress the harmful interaction between electrode materials and electrolytes for lithium ion batteries.[11–13] The alumina coating for lithium cobalt fluorophosphate was reported to prevent metal ion dissolution and improve the cycle performance.[14] A widely recognized interpret is that the alumina coating can protect cathode materials from hazardous reaction products such as HF obtained during the charge–discharge process.[15,16] Petnikota has modified FeO, MnO and $Co_2Mo_3O_8$ by coating of graphene oxide for anode application in lithium ion batteries. All of those composites exhibit better electrochemical properties than corresponding pristine batteries.[17–19] Another example is that amorphous carbon coating is used to prevent PC-based electrolytes insert into graphite accompanied by graphite exfoliation.[20,21] For researches of thermal batteries that anode is Li–Si alloy, carbon coating to CoS_2 cathode was reported by Xie to promote electrochemical properties by enhancing the electronic conductivity.[22]

In this paper, considering the higher self-discharge rate at Li–B/CoS_2 system, the carbon coating of CoS_2 is mainly aimed to block dissolved lithium atom react with CoS_2 cathode. Based on above hypothesis, we reported a facile method through pyrolysis reaction of sucrose, to modify CoS_2 with amorphous carbon coating (this composite of carbon and CoS_2 is referred as CoS_2/C hereafter). It has been proved that CoS_2/C was suitable for thermal batteries and successful in reducing self-discharge rate at Li–B/CoS_2 system. Discharge tests indicated that CoS_2/C released higher capacity than pristine CoS_2. Fig. 1 illustrates how the carbon coating influences self-discharge as a physical barrier.

Experimental

Carbon-coated CoS_2 preparation

CoS_2 was powder from State Key Laboratory of Powder Metallurgy which was synthesized by solid-state reaction of cobalt and sulphur powder.[8] To prepare carbon-coated CoS_2, 1 g sucrose ($C_{12}H_{22}O_{11}$) was dispersed in 2 mL pure water. Then, 9 g CoS_2 and sucrose solution were ground together for 1 h to make it been mixed evenly. After drying, the mixture was carbonized in the argon atmosphere for 4 h after heating to 400 °C at a rate of 5 °C min^{-1}.[23–25]

Single cell preparation

Anodes were Li–B alloys strip which were provided by State Key Laboratory of Powder Metallurgy, and synthesized by smelting metal lithium and boron.[26] Mass fraction of lithium for Li–B alloy is 61 wt%. It was punched to disk with a diameter of 17.5 mm. Electrolyte were composed by 50 wt% LiF–LiCl–LiBr eutectic salts (9.2 wt% LiF, 22 wt% LiCl, 68.4 wt% LiBr) and 50 wt% Nano-MgO binder. Cathodes include 80 wt% CoS_2 or CoS_2/C and 20 wt% electrolytes.

The cathode and separator were shaped to stratiform slice together by spreading the corresponding powders in a die, and then suppressing them under a static compaction pressure of 250 MPa. Two types of single cells were prepared to study the electrochemical properties of anode and cathode respectively. Single cells that the anode was superfluous were composed of 0.20 g anode, 0.36 g separator and 0.18 g cathode. While single cells with superfluous cathode were composed of 0.09 g anode, 0.36 g separator and 0.40 g cathode. Single cells with CoS_2/C and pristine CoS_2 cathode were abbreviated as CoS_2/C cell and CoS_2 cell respectively hereafter.

Materials characterization

Microscopic morphology studies were carried by the scanning electron microscope (LEO 1530 Gemini, Zeiss, Germany) at 15 kV. Crystalline structures of samples were characterized by X-ray diffractometer (D/max2550PC, Rigaku, Japan) at a rate of 8° min^{-1} from 10° (2θ) to 90° (2θ) with Cu Kα radiation. Differential scanning calorimetry (DSC) was conducted by a thermal analyzer system (Hengjiu, Beijing) with a heating rate of 10 °C min^{-1} and a 50 ml min^{-1} Ar flow rate. The carbon coating was observed by transmission electron microscopy (Tecnai G2, FEI, USA). Raman spectroscopies were completed by (T64000, Horiba, Japan) and 514 nm light was used for excitation with an intensity of 20 mW. Particle size distribution was measured by laser particle size analysis (Mastersizer3000, Malvern, England).

Electrochemical measurements

Anode, separation-cathode disk were fabricated to single cell. The test was conducted at 520 °C with a fluctuation of 5 °C. Single cells were discharged at constant current and pulse current respectively. In pulse discharge, the current densities were ranged from 100 mA cm^{-2} to 600 mA cm^{-2} for 2 s every 20 s to study total polarization and power properties. Discharge data were obtained by electronic load (ITECH, IT8511, USA). Total polarization was calculated by following formula.[27]

$$R_{total} = \Delta U/\Delta I$$

here R_{total} denotes the total polarization of a single cell. ΔU denotes the voltage drop caused by pulse current. ΔI denotes the difference between pulse current and steady current.

Results and discussion

X-ray diffraction patterns of both CoS_2/C and pristine CoS_2 are shown in Fig. 2a. All peaks of pristine CoS_2 and CoS_2/C can be indexed to a pure-phase, and no apparent differences appear between CoS_2 and CoS_2/C patterns, except the whole diffraction intensity. It indicates that the coating process has no affection on the crystal structure of pristine CoS_2. Besides, no peaks involved to carbon are observed in diffraction patterns of CoS_2/C. Fig. 2b is the results of XRD analysis of Li–B alloy anode. It shows that Li–B alloy was mainly made up of free lithium metal and LiB compound. According to past studies, no free lithium metal was appeared at Li–Si or Li–Al alloy anode. It is the free lithium metal that makes the Li–B alloy has much more activity than that of Li–Si or Li–Al alloy.

Fig. 3a and b display SEM images of pristine CoS_2 and CoS_2/C respectively. Both pristine CoS_2 and CoS_2/C show aggregation which is sticked by tiny spherical particles. There are gaps and holes between tiny spherical particles, which can provide the passageway for molten electrolytes at the process of discharge. Compared Fig. 3a and b, CoS_2/C has bigger granularity than pristine CoS_2. This phenomenon can be explained by bonding of sucrose. Since the melting point of sucrose is 186 °C,[28] sucrose will be heated to the liquid state before the carbonized stage and CoS_2 particles may be bonded by viscous molten sucrose. The changes of granularity observed by SEM are also identical to the consequence of particle size analysis. Median particle diameter (D50) of pristine CoS_2 is increased from 19.7 μm to 26.8 μm after coating. Fig. 3c and d show the TEM micrographs of CoS_2/C particles. There is a clear boundary between the core of CoS_2 and the bright translucent shell materials of the carbon. The thickness is estimated to be 6 nm. The combination between CoS_2 and carbon is proved to be complete, only in this way can carbon shell protect CoS_2 particles effectively.

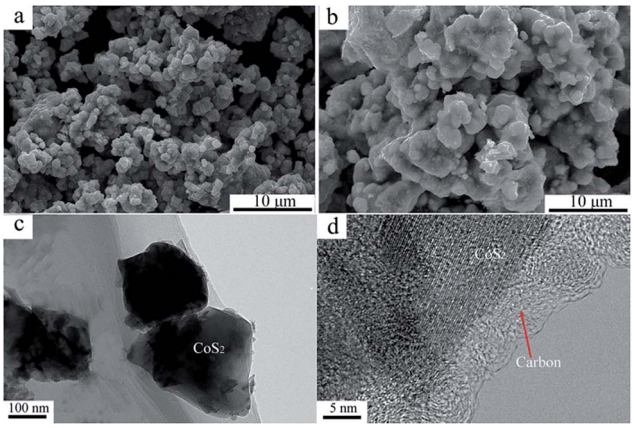

Fig. 3 SEM images of pristine CoS_2 (a) and carbon-coated CoS_2 (b). TEM images of carbon-coated CoS_2 (c, d).

Fig. 4a exhibits the Raman spectroscopy of CoS_2/C. The peaks at 1590 cm^{-1} and 1358 cm^{-1} are commonly referred as G peak and D peak.[29] G peak is corresponding to a Raman active E_{2g} mode of two-dimensional graphite layer, while D peak is attributed to a zone boundary phonon activated by disordered graphite or glass carbon.[30] The ratio of intensity between D peak and G peak (I_D/I_G) is 0.65. A general expression that gives the crystallite size (La) of graphite from the intensity ratio I_D/I_G is given by

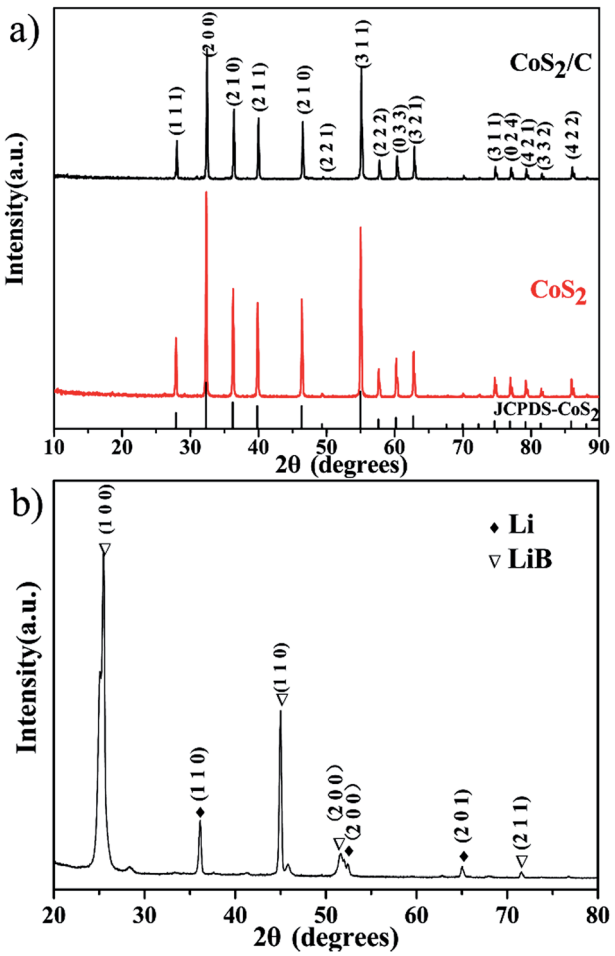

Fig. 2 XRD patterns of CoS_2/C and pristine CoS_2 (a). XRD patterns of Li–B alloy anode (b).

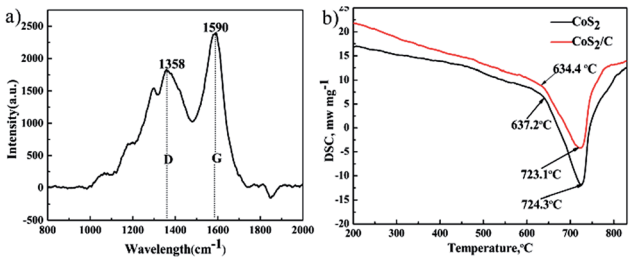

Fig. 4 Raman spectroscopy of CoS_2/C (a). Differential scanning calorimeter of pristine CoS_2 and CoS_2/C (b).

$$\mathrm{La(nm)} = \frac{560}{E_l^4}(I_D/I_G)^{-1},$$

where E_l (2.41 eV) is the excitation laser energy used in the Raman experiment.[31] The La of the carbon coating calculated by this formula is 25.5 nm. It indicates that the carbon coating has considerable graphitic form and desirable electronic conductivity, which is necessary for the high power property at thermal batteries. In addition, no peak related to the C=C fundamental stretching vibration of $S_2C{=}CS_2$ configuration is observed at around 1445 cm^{-1}. It reveals that no polymer is produced among interaction of CoS_2 and sucrose.

Fig. 4b gives results of differential scanning calorimeter of pristine CoS_2 and CoS_2/C. Good thermal stability of cathode materials is a significant requirement at thermal batteries. Sulfide cathode materials with bad thermal stability may decompose and produce sulfur steam because the instantaneous high temperature at the beginning of activation,[32] which leads fatal safe issues and loss of capacity. Only one endothermic peak related to decomposition of CoS_2 is observed in both curves. The endothermic peak of pristine CoS_2 is 724.3 °C, and that of CoS_2/C is 723.1 °C. In addition, approximate endothermic onset temperature that sample become decompose are pointed at two curves. DSC date can be inferred that the carbon coating has no apparent influence on the thermal stability of pristine CoS_2.

According to the past studies, the discharge reactions of CoS_2 included three steps which are expressed by following chemical reaction equations.[1,33]

$$(1-x)\mathrm{CoS_2} + (2-4x)\mathrm{e^-} \rightarrow \mathrm{Co_{(1-x)}S} + (1-2x)\mathrm{S^{-2}} \quad (1)$$

$$\mathrm{Co_{(1-x)}S} + \frac{2+16x}{9}\mathrm{e^-} \rightarrow \frac{1-x}{9}\mathrm{Co_9S_8} + \frac{1+8x}{9}\mathrm{S^{-2}} \quad (2)$$

$$\mathrm{Co_9S_8} + 16\mathrm{e^-} \rightarrow 9\mathrm{Co^0} + 8\mathrm{S^{-2}} \quad (3)$$

Correspondences of reaction equations are three plateau voltages. V. A. Bryukin inferred that x was ranged from 0.110 to 0.124.[34] calculated by the theories of V. A. Bryukin, the specific capacity of first discharge plateau is 374–382 mA h g^{-1}, that of second and third discharge plateau are 102–110 mA h g^{-1} and 348 mA h g^{-1} respectively.

Once a thermal battery is activated at the high temperature, self-discharge caused by dissolved lithium anode is remarkable. Thus, on the open circuit, the electromotive force (EMF) of the single cell will be decreased as time goes on due to active electrode materials are lost gradually by self-discharge reaction. Fig. 5a clarifies the relation between EMF and time of the battery cells fabricated with CoS_2 and CoS_2/C cathodes on the open circuit at 520 °C (single cells are designed with superfluous anode materials). EMF-time curves in the Fig. 5a reveal that active cathode materials are exhausted at last. There is no doubt that EMF of CoS_2/C cell is decreased more slowly than that of pristine CoS_2 cell. It can be concluded that CoS_2/C cell has lower self-discharge rate than pristine CoS_2 cell. Multiple EMF plateaus in the Fig. 5a represent phase transition of cathode materials. According to discharge process of CoS_2, three open-circuit plateau voltages ordered from the most to the least are related to phases of CoS_2, $Co_{1-x}S$, Co_9S_8 respectively. Fig. 5b shows differential capacity plots of cells. Three peaks located at 1.93 V, 1.80 V, 1.57 V in differential capacity plots are also very consistent with open circuit voltage curves. The EMF of the reaction from CoS_2 to $Co_{1-x}S$ has been depressed by carbon coating.

In order to further validate above deductions, X-ray diffraction was applied for analyzing the composition of the cathode part which has experienced an open circuit losses. To prepare appropriate samples for XRD, CoS_2/C cell and pristine CoS_2 cell were laid on open circuit for 40 min at 520 °C respectively. Then, cathode parts were rinsed with distilled water to remove electrolytes which will produce obvious interference signal. Fig. 6 displays XRD results of remainder active cathode materials which are obtained during open circuit. Diffraction spectrums show that the major phases of two samples are CoS_2 and $Co_{1-x}S$. Peaks located at 32.39° (P1) and 35.18° (P2) are contributed to CoS_2 and $Co_{1-x}S$ respectively. The mass ratio of CoS_2 and $Co_{1-x}S$ on the samples is directly proportional to intensity ratio of P1 and P2 (P1/P2), and the P1/P2 of CoS_2/C cell is 0.83, while for pristine CoS_2 is 0.14. Thus we can get the conclusion that there are less lost active materials on CoS_2/C cell. Those results are consistent with the analysis of the EMF curve in Fig. 5a. It should be noted that obvious peaks related to Co_9S_8 and Co_3S_4 appear at two patterns. Co_9S_8 phase may exist because of the non-uniform distribution of self-discharge reaction. A small amount of Co_3S_4 can be related to thermal decomposition of CoS_2.[35]

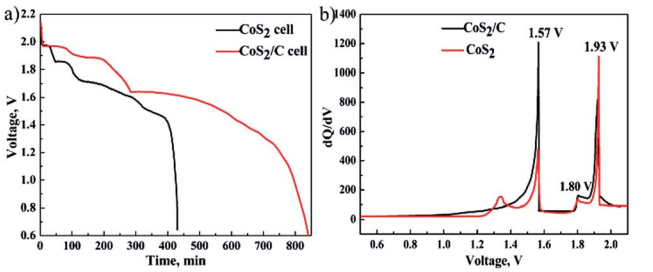

Fig. 5 The voltage of single cells as function of time on open circuit at 520 °C (a). Differential capacity plots of CoS_2/C cell and pristine CoS_2 (b).

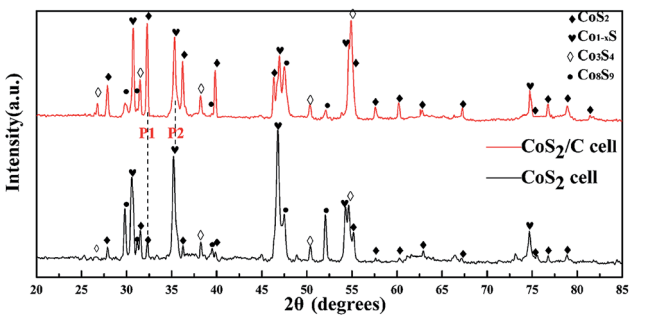

Fig. 6 XRD pattern of cathode electrode materials after 40 min on open circuit losses at 520 °C.

Fig. 7 reports discharge curve of single cell that Li–B alloy anode is superfluous at 100 mA cm^{-2} (a) and 500 mA cm^{-2} (b). It can be used to study electrochemical properties of cathode materials. Because only the capacity of first discharge plateau for CoS_2 is utilized at practice application, specific capacity of first discharge plateau is regarded as standard to compare discharge capability of CoS_2 cathode. Fig. 7a reveals that the specific capacity of first discharge plateau for CoS_2/C is 243 mA h g^{-1}, which is 50 mA h g^{-1} higher than of pristine CoS_2, and accounts for 64.9% of the theoretical capacity of CoS_2 (374 mA h g^{-1}). In Fig. 7b, the specific capacity for first discharge plateau of CoS_2/C and pristine CoS_2 are 283 mA h g^{-1} and 258 mA h g^{-1}, respectively. CoS_2/C cells perform more flat and long first voltage plateau than pristine CoS_2 cell. The carbon coating has a significant effect in increasing specific capacity whether at 500 mA cm^{-2} or 100 mA cm^{-2}. However, due to the loss of capacity caused by self-discharge will increase with discharge time, and completing discharge takes a longer time at 100 mA cm^{-2} than at 500 mA cm^{-2}, CoS_2/C with lower self-discharge represents a more obvious advantage when single cells are discharged at the low current rate of 100 mA cm^{-2}.

Sustained self-discharge reactions will consume lithium from anode. Thus self-discharge rate at cathode has a great influence on the specific capacity of Li–B alloy anode. To compare the specific capacity of Li–B alloy anodes which are matched with different cathodes, single cells that cathode is superfluous are discharged at 100 mA cm^{-2} (Fig. 8a) and 500 mA cm^{-2} (Fig. 8b). In the Fig. 8a, as a result of using CoS_2/C cathode, the specific capacity of Li–B anode is increased from 805 mA h g^{-1} to 885 mA h g^{-1} at first plateau. In the Fig. 8b, an

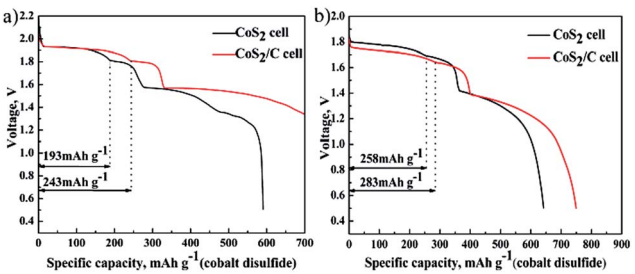

Fig. 7 Specific discharge capacity of cobalt disulfide cathode, data of pristine CoS_2 cell or CoS_2/C cell at 100 mA cm^{-2} (a) and 500 mA cm^{-2} (b).

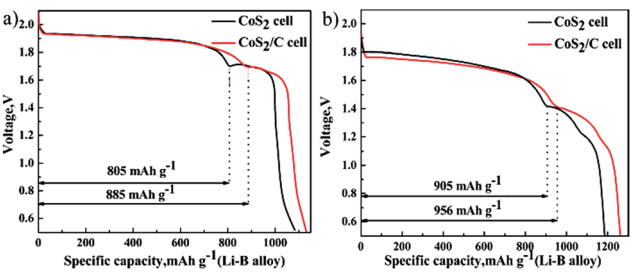

Fig. 8 Specific discharge capacity of Li–B alloy anode, data of pristine CoS_2 cell or CoS_2/C cell at 100 mA cm^{-2} (a) and 500 mA cm^{-2} (b).

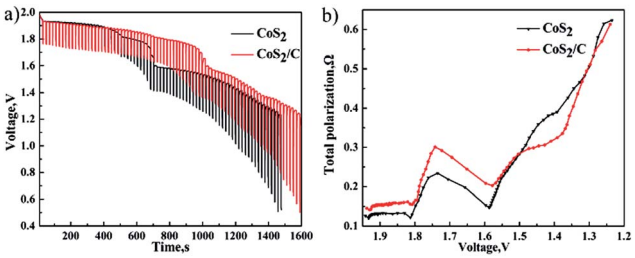

Fig. 9 Discharge performance at a background current of 100 mA cm^{-2} and pulse current of 600 mA cm^{-2} for 2 s every 20 s (a). Comparison of total polarization between CoS_2 cell and CoS_2/C cell (b).

increase of 51 mA h g^{-1} also appears on first discharge plateau of Li–B alloy anode. There is no doubt that CoS_2/C cathode improves discharge efficient of Li–B alloy anode. The consequences of Fig. 8 provide further evidence that carbon coating on the CoS_2 has evident effect in depressing self-discharge to the Li–B/LiF–LiCl–LiBr/CoS_2 cells. Li–B alloy is made up of lithium and LiB compound, which results in first and second discharge plateaus respectively.[36] Besides, only lithium metal can dissolve into electrolytes and cause self-discharge. Therefore, CoS_2/C cathode only has positive influence on the first discharge plateau of Li–B alloy anode.

In Fig. 7a and 8a, the first plateau voltage of CoS_2/C cell is equal to pristine CoS_2 cell at 100 mA cm^{-2}. In Fig. 7b and 8b, compared with pristine CoS_2 cell, however, a decrease about 0.4 V to the plateau voltage appears at CoS_2/C cell when the current density is increased to 500 mA cm^{-2}. Apparently, the carbon coating also has blocked diffusion of lithium ion, which produces additional concentration polarization for single cells at 500 mA cm^{-2}. The unique porous structure of amorphous carbon provide channels for the diffusion of lithium ion, which ensures enough lithium ion will diffuse to reaction interface in time at the low current density, but not at the high current density of 500 mA cm^{-2}. To know the detail of polarization increased by the carbon coating and estimate properties of single cell at transitory high current, single cells were discharged at pulse loading mode. Fig. 9a depicts pulse discharge curve. The total polarization was calculated by previous formula. Fig. 9b compares the difference of total polarization between CoS_2 cell and CoS_2/C cell. The resistances of both cells are increased with discharge time. Though CoS_2/C cell shows higher total polarization than CoS_2 cell especially when the voltage is higher than 1.65 V. CoS_2/C cell also exhibits excellent performances at pulse current, which meets the requirement of delivering electricity with high power for thermal batteries.

Conclusions

In summary, to solve self-discharge problem at Li–B/LiF–LiCl–LiBr/CoS_2 system, we have modified CoS_2 with carbon coating by facile pyrolysis reaction of sucrose. Compare to the CoS_2/Li–B couple, thermal batteries fabricated with CoS_2/C and Li–B alloy can deliver much higher specific capacity. The enhanced

discharge efficiency can be explained by the mechanisms that the carbon coating can prevent CoS_2 from directly exposing to the electrolytes and minimize the self-discharge reactions between the cathode and dissolved lithium. Besides, the carbonized process has no obvious influences on the thermal stability of pristine CoS_2. It has been proved that CoS_2/C was efficient and safe cathode materials. CoS_2/C has great merits and value particularly at the long-life thermal batteries for the low self-discharge rate. The method of modifying cathode materials with carbon may be applied to other cathode materials such as FeS_2 and NiCl for thermal batteries, all of those studies are underway.

Conflicts of interest

There are no conflicts of interest to declare.

Acknowledgements

This research work was financially supported by the National Natural Science Foundation of China (51771236), the Innovation-Driven Project of Central South University (No. 2017CX002).

References

1 R. A. Guidotti and P. Masset, *J. Power Sources*, 2006, **161**, 1443–1449.
2 K. Nitta, S. Inazawa, S. Sakai, A. Fukunaga, E. Itani and K. Numata, *SEI Tech. Rev.*, 2013, **76**, 33–39.
3 P. Kulkarni, S. K. Nataraj, R. G. Balakrishna, D. H. Nagarajua and M. V. Reddy, *J. Mater. Chem. A*, 2017, **5**, 22040–22094.
4 M. Chen, X. Yin, M. V. Reddy and S. Adams, *J. Mater. Chem. A*, 2015, **3**, 10698–10702.
5 S. Fujiwara, M. Inaba and A. Tasaka, *J. Power Sources*, 2010, **195**, 7691–7700.
6 R. A. Guidotti and P. Masset, *J. Power Sources*, 2008, **183**, 388–398.
7 A. J. Burak and M. F. Simpson, *JOM*, 2016, **68**, 1–7.
8 N. Watanabe, K. Nakanishi and A. Komura, *Journal of the Society of Chemical Industry Japan*, 1968, **71**, 1599–1602.
9 J. X. Gao, *Microcosmic characteristics and discharge properties of cobalt sulfide as cathode in thermal batteries*, Central South University, 2014.
10 P. Zeng, *Dissolution characteristics and discharge properties of LiB alloys as anode in thermal batteries*, Central South University, 2016.
11 F. Wu, Q. Xue, L. Li, X. Zhang, Y. Huang and E. Fan, *RSC Adv.*, 2017, **7**, 1191–1199.
12 P. R. Kumar, V. Madhusudhanrao and B. Nageswararao, *J. Solid State Electrochem.*, 2016, **20**, 1855–1863.
13 M. V. Reddy, G. V. Subba Rao and B. V. Chowdari, *Chem. Rev.*, 2013, **113**, 5364–5457.
14 S. Amaresh, K. Karthikeyan and K. J. Kim, *RSC Adv.*, 2014, **4**, 23107–23115.
15 M. Seungtaek, I. Kentarou and K. Shinichi, *J. Mater. Chem.*, 2005, **17**, 3695–3704.
16 M. Yoshio, H. Wang and K. Fukuda, *J. Electrochem. Soc.*, 2000, **147**, 1245–1250.
17 S. Petnikota, S. K. Marka, A. Banerjee, M. V. Reddy, V. V. S. S. Srikanth and B. V. R. Chowdari, *J. Power Sources*, 2015, **293**, 253–263.
18 S. Petnikota, V. V. S. S. Srikanth, P. Nithyadharseni, M. V. Reddy, S. Adams and B. V. R. Chowdari, *ACS Sustainable Chem. Eng.*, 2015, **3**, 3205–3213.
19 S. Petnikota, S. K. Marka, V. V. S. S. Srikanth, M. V. Reddy and B. V. R. Chowdari, *Electrochim. Acta*, 2015, **178**, 699–708.
20 L. Wang, Z. Liu, Q. Guo, X. Guo and J. Gu, *RSC Adv.*, 2017, **7**, 36735–36743.
21 S. Petnikota, N. K. Rotte, V. V. S. S. Srikanth, B. S. R. Kota, M. V. Reddy and K. P. Loh, *J. Solid State Electrochem.*, 2014, **18**, 941–949.
22 S. Xie, Y. Deng and J. Mei, *Electrochim. Acta*, 2017, **231**, 287–293.
23 S. Amaresh, K. Karthikeyan and I. C. Jang, *J. Mater. Chem. A*, 2014, **2**, 11099–11106.
24 J. Dong, D. Li and Z. Peng, *J. Solid State Electrochem.*, 2008, **12**, 171–174.
25 J. Wang and X. Sun, *Energy Environ. Sci.*, 2012, **5**, 5163–5185.
26 Z. J. Liu, Z. Y. Li, W. Duan, X. H. Qu, B. Y. Huang and S. Q. Zhang, *J. Mater. Sci. Technol.*, 2000, **16**, 581–584.
27 S. Xie, Y. Deng, J. Mei, Z. Yang, W. M. Lau and H. Liu, *Composites, Part B*, 2016, **93**, 203–209.
28 M. Hurtta, I. Pitkänen and J. Knuutinen, *Carbohydr. Res.*, 2004, **339**, 2267–2273.
29 J. Schwan, S. Ulrich and V. Batori, *J. Appl. Phys.*, 1996, **80**, 440–447.
30 A. C. Ferrari and J. Robertson, *Phys. Rev. B: Condens. Matter Mater. Phys.*, 2008, **61**, 14095–14107.
31 L. G. Cancado, K. Takai and T. Enoki, *Appl. Phys. Lett.*, 2006, **88**, 163106.
32 S. Serge, *J. Power Sources*, 2005, **142**, 361–369.
33 Y. Wang, J. Wu, Y. Tang, X. Lu, C. Yang and M. Qin, *ACS Appl. Mater. Interfaces*, 2012, **4**, 4246–4250.
34 V. A. Bryukvin and L. I. Blokhina, *Nickel-Cobalt International 97 Symposium*, Canada, August 1997.
35 M. A. Rodriguez, E. N. Coker, J. J. M. Griego, C. D. Mowry, A. S. Pimentel and T. M. Anderson, *Powder Diffr.*, 2016, **31**, 90–96.
36 P. Sanchez, C. Belin, G. Crepy and A. D. Guibert, *J. Mater. Sci.*, 1992, **27**, 240–246.

